

Revealing the hidden paleomagnetic information from the airborne total magnetic intensity (TMI) data

Michael S. Zhdanov^{1,2*}, Michael Jorgensen^{1,2} and John Keating³ demonstrate that the remanent magnetisation of rocks can be determined remotely from the airborne magnetic data, opening up the possibility of paleomagnetic study on a large scale without extracting specific rock samples from the ground.

Introduction

Earth's magnetic field is a vector field characterised by both amplitude and direction, and it is a vector function of the coordinates of the observation point (horizontal and vertical coordinates). Conventional airborne, ground, and marine magnetic surveys, however, collect the amplitude of the magnetic field only, or Total Magnetic Intensity (TMI), which is a scalar field.

Until recently, the interpretation of the TMI data was based on different types of transformation of this field and the qualitative analysis of the resulting maps. The first step of TMI data interpretation usually involves the calculation of the anomalous magnetic intensity (AMI) field by subtracting the scalar intensity of the earth's magnetic field, usually represented by the International Geomagnetic Reference Field (IGRF). The most widely used transformations of the AMI data include different derivatives of the magnetic field intensity, reduction to the pole (RTP) and the equator (RTE), residual field calculations, and upward and downward analytical continuations (Blakely, 1995). The maps of the transformed magnetic field provide useful qualitative information about the main geological features of the survey area, like locations of magnetic anomalies, geological strike directions, major geological faults, and edges of the different geological formations, etc.

The methods of magnetic field inversion developed over the last decades resulted in a paradigm change in the interpretation of the TMI data (e.g., Li and Oldenburg, 1996; Portniaguine and Zhdanov, 2002). These methods invert for magnetic susceptibility, linking induced magnetisation to the Earth's magnetic field. 3D images of the subsurface magnetic susceptibility distribution help us to identify the locations of the rock formations with anomalous magnetisation, thus providing information about zones of potential mineralisation. These methods have become widely used in the quantitative interpretation of the magnetic survey data.

However, conventional inversion methods for Total Magnetic Intensity (TMI) data assume that rocks do not possess remanent magnetisation, attributing the observed magnetic field solely to induced magnetisation. In fact, rocks exhibit both induced and remanent magnetisations, preserving the historical Earth's magnetic field at their time of formation.

Two primary natural mechanisms contribute to remanent magnetisation. First, in igneous rocks, as magnetic minerals cool through the Curie point, their magnetic domains align with the Earth's magnetic field during formation, creating a lasting record of orientation. The second mechanism occurs during sedimentation, where tiny grains in sedimentary deposits align with the Earth's magnetic field during deposition before the rock consolidates.

The remanent magnetisation is characterised by magnetic vectors recorded in rock. It plays a critical role in paleomagnetic applications, such as magnetostratigraphy, paleointensity studies, and apparent polar wander. Remanent magnetisation is also used to investigate sedimentary, igneous, and metamorphic rocks (Tauxe, 2003).

The vector of remanent magnetisation can be described by its inclination, declination, and intensity. Until recently, these parameters were determined from paleomagnetic samples in the labs only using specific laboratory procedures, including measurements and demagnetisation, which are very laborious and time-consuming.

In this paper, we demonstrate that the remanent magnetisation of the rocks can be determined remotely from the airborne magnetic data. This opens the possibility of paleomagnetic study on a large scale without extracting specific rock samples from the ground.

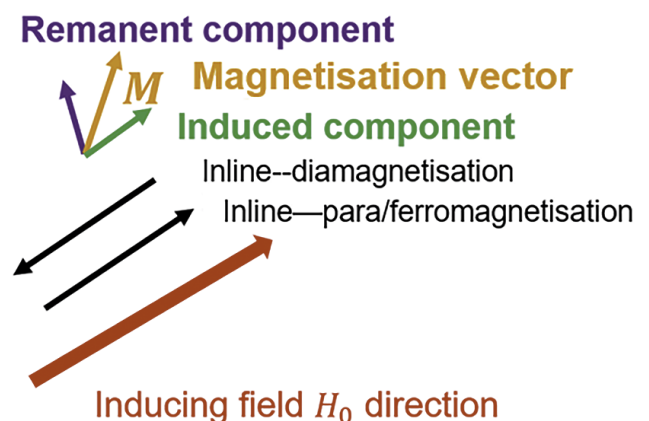


Figure 1 Representation of magnetisation vector as a superposition of remanent and induced magnetisation (after Jorgensen et al., 2023).

¹ TechnoImaging | ²The University of Utah | ³PJX Resources Inc

* Corresponding author, E-mail: mzhdanov@technoimaging.com

DOI: 10.3997/1365-2397.fb2024060

Induced and remanent magnetisations

In a general case, the total magnetisation vector, \mathbf{M} can be represented as a superposition of induced, \mathbf{M}_{ind} , and remanent, \mathbf{M}_{rem} , magnetisations (Figure 1):

$$\mathbf{M}(\mathbf{r}) = \mathbf{M}_{ind}(\mathbf{r}) + \mathbf{M}_{rem}(\mathbf{r}). \quad (1)$$

The induced magnetisation is parallel and linearly proportional to the inducing magnetic field, \mathbf{H}_0 , $\mathbf{M}_{ind}(\mathbf{r}) = \chi(\mathbf{r})\mathbf{H}_0$, where $\chi(\mathbf{r})$ is the magnetic susceptibility.

We should note that paramagnetic and ferromagnetic materials tend to align in the direction of the inducing field, while diamagnetic materials tend to align in the opposite direction (Figure 1).

The remanent magnetisation can manifest itself as a vector pointing away from the inducing field (Figure 1):

$$\mathbf{M}_{rem}(\mathbf{r}) = \{R_x(\mathbf{r}), R_y(\mathbf{r}), R_z(\mathbf{r})\}, \quad (2)$$

where $\{R_x(\mathbf{r}), R_y(\mathbf{r}), R_z(\mathbf{r})\}$ are the scalar components of the remanent magnetisation.

In recent decades, there has been considerable focus in research and applications on extracting magnetisation vectors from observed Total Magnetic Intensity (TMI) data, as evidenced by studies such as those by Ellis et al. (2012), Zhu et al. (2015), Li (2017), Jorgensen and Zhdanov (2021), and Jorgensen et al. (2023). Numerous developed methods have concentrated on inverting TMI data to reveal the distribution of the underground magnetisation vector (Magnetisation Vector Inversion – MVI).

However, as Figure 1 shows, the magnetisation vector is a superposition of the induced and remanent magnetisation, which makes it challenging to extract the remanent magnetisation using MVI. We propose a rigorous approach by simultaneously inverting TMI data to reveal both the induced and remanent components of the magnetisation vector. To address the non-uniqueness inherent in the inverse problem, we incorporate Gramian regularisation (Zhdanov, 2015, 2023).

The studies conducted by Zhu et al. (2015) and Jorgensen and Zhdanov (2021) illustrated the viability of obtaining a dependable solution to the inverse problem related to the magnetisation vector by strengthening correlations among its various components. We suggest applying this additional constraint specifically to the components of the remanent magnetisation. This can be achieved by minimising the following Gramian stabilisers,

$$S_{G\beta}(\mathbf{m}) = \left| \begin{matrix} (\mathbf{R}_\beta, \mathbf{R}_\beta) & (\mathbf{R}_\beta, \chi) \\ (\chi, \mathbf{R}_\beta) & (\chi, \chi) \end{matrix} \right| = \min, \quad \beta = x, y, z; \quad (3)$$

where \mathbf{R}_β is the vector of discrete values of the β component of remanent magnetisation, and χ is the vector of discrete values of magnetic susceptibility formed by their values in every cell. Symbol (\dots, \dots) denotes the L2 inner product operation (Zhdanov, 2015).

To mitigate uncertainty regarding the contributions of induced and remanent magnetisation to the total field, we can integrate prior information about magnetic susceptibility, χ_{apr} , into the inversion process. This can be achieved by imposing the following constraint:

$$S_\chi(\mathbf{m}) = \|\chi - \chi_{apr}\|^2 = \min; \quad (4)$$

Thus, the parametric functional for the regularised solution of the inverse problem takes the following form:

$$P^\alpha(\mathbf{m}) = \phi(\mathbf{m}) + \alpha c_1 S_\chi(\mathbf{m}) + \alpha c_2 \sum_{\beta=x,y,z} S_{G\beta}(\mathbf{m}) = \min, \quad (5)$$

where $\phi(\mathbf{m})$ is a data misfit term, α is a regularisation parameter, and coefficients c_1, c_2 balance the stabilisers. The parametric functional is minimised through a reweighted regularised conjugate gradient scheme, as outlined by Zhdanov (2015). In cases where no prior susceptibility information is available in the region, χ_{apr} is established by conducting an inversion solely for susceptibility first, which is subsequently employed as a soft constraint.

Analysis of TMI data collected over a Sullivan-style massive sulphide target near the historical Estella Mine in British Columbia, Canada

PJX Resources Inc., a Toronto-based Canadian exploration company, recently discovered sediment hosted semi-massive to massive sulphide boulders near the historical Estella Mine in British Columbia, Canada, exhibiting Sullivan deposit-style and grade zinc, lead, silver, cadmium, and indium magnetisation. This is the first Sullivan-style and grade discovery of this kind outside the Sullivan deposit area in more than a century. The sulphide boulders with zinc (sphalerite mineral), lead (galena), and iron (pyrite and pyrrhotite) are magnetic.

PJX’s Dewdney Trail property in this study was surveyed in May 2021 using a helicopter-borne MobileMT, VLF-EM, and magnetic system by Expert Geophysics Limited of Aurora, Ontario, Canada. The survey was flown with a Eurocopter AS 350 B3 at an average survey speed of 12 m/sec, average terrain clearance of 195 m, average magnetometer clearance of 116 m, and an average EM sensor clearance of 98 m.

In total, 895 line-km of TMI data, flown at 100 m spacing, were inverted using the developed method incorporating a GPU-accelerated inversion algorithm with a moving sensitivity domain (Cuma and Zhdanov, 2014; Jorgensen and Zhdanov, 2021). The concept of the moving sensitivity domain approach can be described as follows (Cox and Zhdanov, 2008; Zhdanov, 2018). For a given receiver (magnetic sensor), we compute and store the sensitivities for those inversion cells within a predetermined horizontal distance from this receiver, i.e., the sensitivity domain. The radius of the sensitivity domain is based on the rate of sensitivity attenuation. Typically, the size of the sensitivity domain is less than the size of an airborne survey. The size of the sensitivity domain for the magnetic field is proportional to $1/r^3$, where \mathbf{r} is the distance from a given receiver. The sensitivity matrix for the entire 3D earth model could be constructed as the superposition of the sensitivity domains from all receivers in the survey area. This approach helps to reduce the required computer memory and speed up the computations dramatically.

Figure 2 shows the map of the observed TMI data over the airborne survey area.

The TMI data were inverted to magnetic, susceptibility and remanent magnetisation vector models on a detailed fine grid

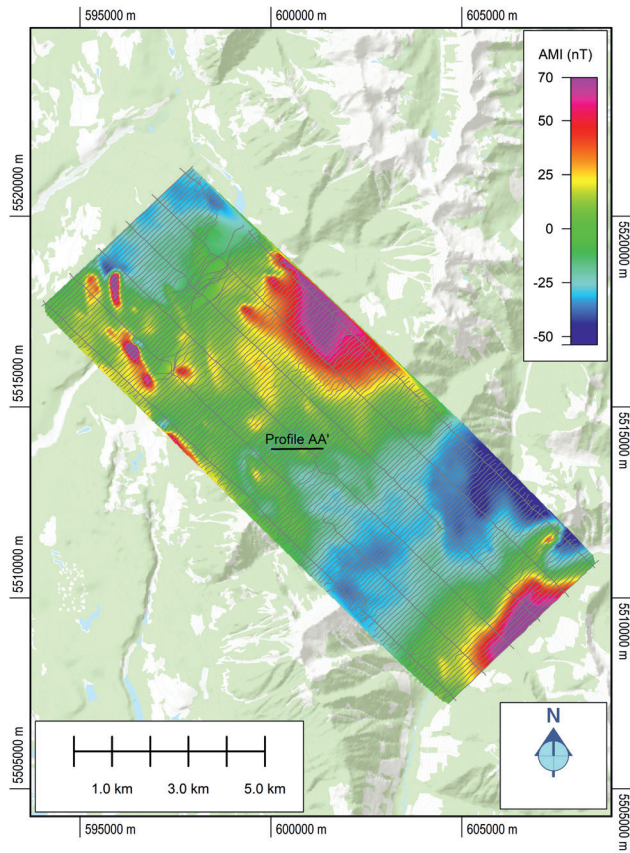


Figure 2 The map of the observed TMI data over the airborne survey area.

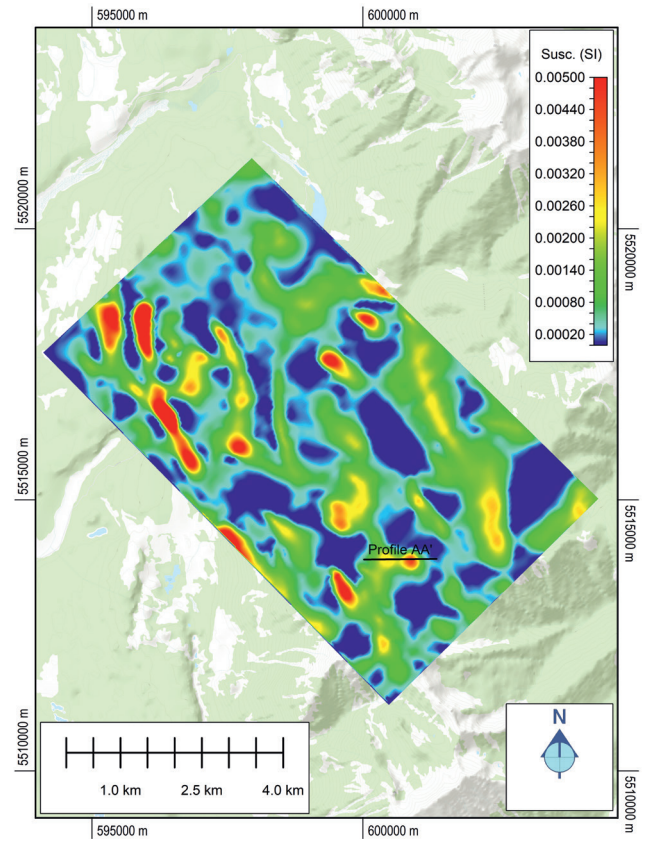


Figure 3 The horizontal section of the inverse magnetic susceptibility model at a depth of 150 m. The bold black line shows the profile crossing the Sullivan-style target area near the historical Estella Mine.

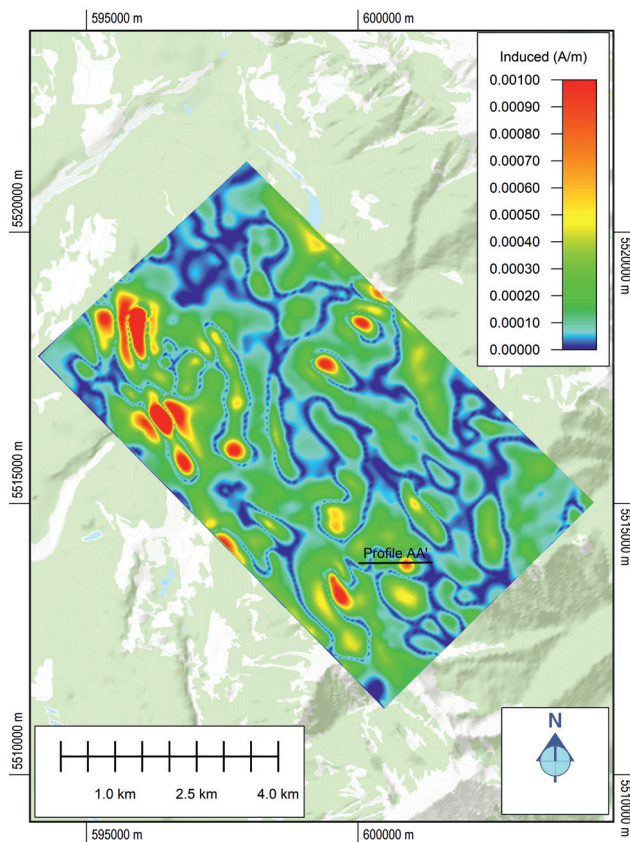


Figure 4 The horizontal section of the amplitude of the induced magnetisation model at a depth of 150 m. The bold black line shows the profile crossing the Sullivan-style target area near the historical Estella Mine.

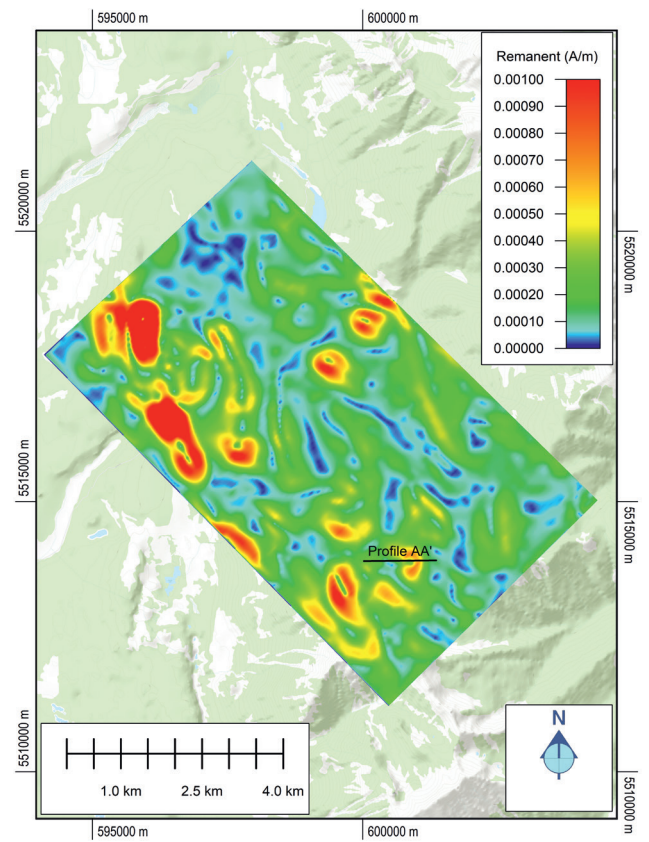


Figure 5 The horizontal section of the amplitude of the remanent magnetisation model at a depth of 150 m. The bold black line shows the profile crossing the Sullivan-style target area near the historical Estella Mine.

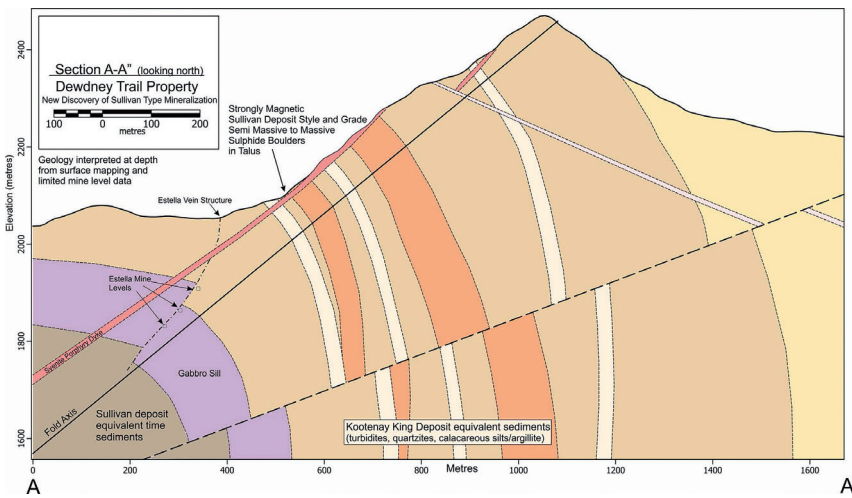


Figure 6 Geological cross-section of the Sullivan-style target area near the historical Estella Mine along the profile shown by the black line in Figures 3, 4, and 5 (looking north).

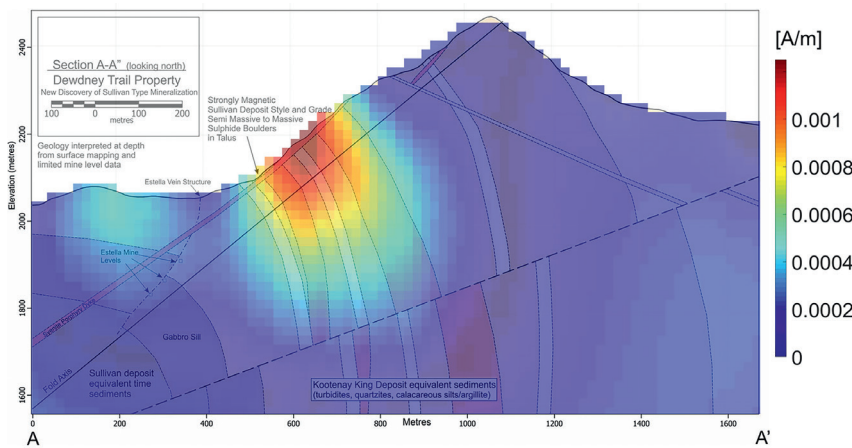


Figure 7 The vertical section of the induced magnetisation model superimposed over the geological cross-section of the Sullivan-style target area near the Estella Mine along the profile shown by the black line in Figures 3, 4, and 5.

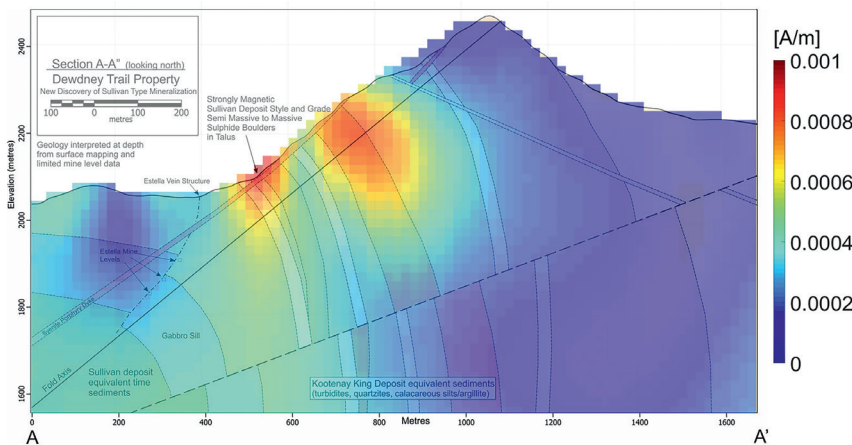


Figure 8 The vertical section of the remanent magnetisation model superimposed over the geological cross-section of the Sullivan-style target area near the Estella Mine along the profile shown by the black line in Figures 3, 4, and 5.

discretisation of 10 x 20 m laterally with a logarithmic vertical discretisation to the depth of 2.6 km.

Figure 3 presents the horizontal section at a depth of 150 m of the inverse magnetic susceptibility model. Figures 4 and 5 show the horizontal sections at a depth of 150 m of the amplitudes of the induced and remanent magnetisation models, respectively. The bold black line in these figures indicates the profile crossing the Sullivan style target area near the historical Estella Mine, which will be analysed in detail below.

In Figure 6, we show a geologic cross-section of the target area interpreted from surface mapping and limited underground Estella mine data. Figures 7 and 8 represent the induced and remanent mag-

netisation models superimposed over the geologic cross-section. The sulphide boulders with pyrrhotite likely to have belonged to the horizon imaged in red in Figure 7. However, the two anomalies in red in Figure 8 identify the potential for separate magnetic horizons with mineralisation. The possibility of multiple mineralised horizons is similar to what occurs at the Sullivan deposit. The low magnetic signature between the two red anomalies coincides with non-magnetic mineralisation (predominantly sphalerite with minor pyrrhotite) in the outcrop that is located about 100 m north of the section. The non-magnetic mineralisation is only visible because erosion has created a window through a thin alkalic porphyry dyke that is masking a potential deposit beneath the dyke.

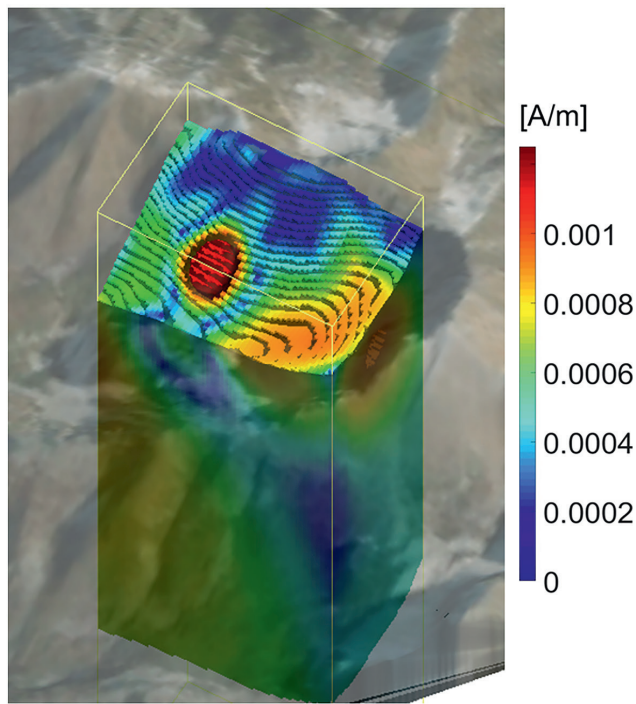


Figure 9 3D column of the induced magnetisation model near the Estella Mine. The red isobody may correspond to the bedrock source of the high pyrrhotite boulders.

Figures 9 and 10 show three-dimensional columns of the induced and remanent magnetisation models, respectively.

The red isobody in Figure 9 clearly delineates a possible source of the magnetic boulders observed downslope with high pyrrhotite content, clearly generating the induced magnetic response. However, Figure 10 provides a more complete picture of the geology of the area —delineating a broad feature relating to potentially multiple stacked mineralised sedimentary horizons. This would be consistent with the multiple styles of magnetic and non-magnetic mineralisation discovered in boulders and outcrop. Multiple stacked mineralised horizons are also similar to what occurs at the Sullivan deposit. The model also suggests that the mineralisation may plunge to the south along stratigraphy.

Conclusions

Conventional total magnetic intensity (TMI) data inversion algorithms generate a distribution of the magnetic susceptibility in the subsurface. This paper explores a unique method for extracting the remanent magnetisation from observed TMI field data. This approach involves representing the magnetisation vector as a combination of induced magnetisation, aligned parallel to the inducing magnetic field, and remanent magnetisation, positioned arbitrarily in relation to the inducing field. The inversion process targets four unknown scalar parameters — magnetic susceptibility and three scalar components of the remanent magnetisation vector. All four parameters are simultaneously inverted, revealing the comprehensive structure of the rock's magnetic properties. This is significant because remanent magnetisation reflects the historical Earth's magnetic field, which was present during the formation of igneous or sedimentary rocks and was preserved over time. The orientation and intensity of remanent magnetisation indicates the displacement of rock formations by tectonic forces, providing a

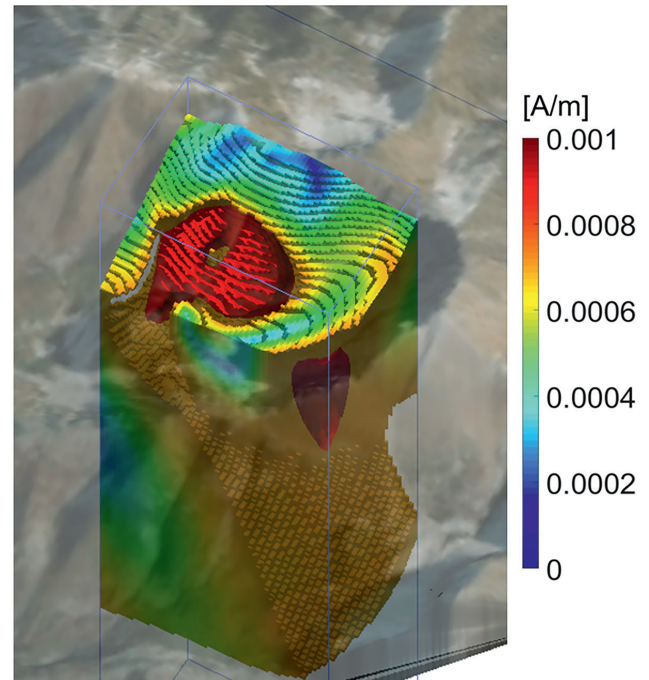


Figure 10 3D column of the remanent magnetisation model near the Estella Mine. The broad red isobody may more accurately reflect the potential for multiple mineralized horizons underlying the thin alkalic intrusive dyke.

more accurate representation of complex geology compared to magnetic susceptibility alone.

We validated this novel approach using the TMI data collected over a Sullivan-style massive sulphide target near the historical Estella Mine in British Columbia, Canada. The direct reconstruction of induced and remanent magnetisation, coupled with the simultaneous recovery of magnetic susceptibility and remanent magnetisation, provides crucial geological and mineralisation insights within the surveyed area.

Acknowledgements

The authors acknowledge the support of the Consortium for Electromagnetic Modelling and Inversion (CEMI) at The University of Utah and TechnoImaging for this research project. We also thank PJX Resources Inc. for permission to publish and Expert Geophysics for gathering high-quality data.

References

- Blakely, R.J. [1995], *Potential theory in gravity and magnetic applications*: Cambridge University Press.
- Cox, L.H. and Zhdanov, M.S. [2008]. Advanced computational methods of rapid and rigorous 3-D inversion of airborne electromagnetic data: *Communications in Computational Physics*, **3**(1), 160-179.
- Cuma, M. and Zhdanov, M.S. [2014]. Massively parallel regularized 3D inversion of potential fields on CPUs and GPUs: *Computers and Geosciences*, **62**, 80-87.
- Ellis, R.G., De Wet, B. and Macleod, I.N. [2012]. Inversion of magnetic data from remanent and induced sources: *22nd ASEG Geophysical Conference and Exhibition, Brisbane, Australia, Expanded Abstracts*.
- Jorgensen, M. and Zhdanov, M.S. [2021]. Recovering magnetization of rock formations by jointly inverting airborne gravity gradiometry and total magnetic intensity data: *Minerals*, **11**, 366.

- Jorgensen, M., Zhdanov, M.S. and Parsons, B. [2023]. 3D Focusing inversion of full tensor magnetic gradiometry data with Gramian regularization: *Minerals*, **13**, 851.
- Li, Y. [2017]. From susceptibility to magnetization: advances in the 3D inversion of magnetic data in the presence of significant remanent magnetization: *Proceedings of Exploration 17: Sixth Decennial International Conference on Mineral Exploration*, 239-260.
- Li, Y. and Oldenburg, D. [1996]. 3-D inversion of magnetic data: *Geophysics*, **61**, 394-408.
- Portniaguine, O. and Zhdanov, M.S. [2002]. 3-D magnetic inversion with data compression and image focusing: *Geophysics*, **67**, 1532-1541.
- Tauxe, L. [2003]. *Paleomagnetic principles and practice*: Kluwer Academic Publishers.
- Zhdanov, M.S. [2015]. *Inverse theory and applications in geophysics*: Elsevier.
- Zhdanov, M.S. [2018]. *Foundations of geophysical electromagnetic theory and methods*: Elsevier.
- Zhdanov, M.S. [2023]. *Advanced methods of joint inversion and fusion of multiphysics data*: Springer Nature.
- Zhu, Y., Zhdanov, M.S. and Cuma, M. [2015]. Inversion of TMI data for the magnetization vector using Gramian constraints: *85th Annual International Meeting, SEG, Expanded Abstracts*, 1602-1606.